Structure of Transmembrane AMPA Receptor Regulatory Protein Subunit γ2

W. Dylan Hale[1,2§], Alejandra Montaño Romero[1,2§], Richard L. Huganir[1,3*], & Edward C. Twomey[1,2,4,5*]

[1]Solomon H. Snyder Department of Neuroscience, Johns Hopkins University School of Medicine, Baltimore, MD USA

[2]Department of Biophysics and Biophysical Chemistry, Johns Hopkins University School of Medicine, Baltimore, MD USA

[3]Kavli Neuroscience Discovery Institute, Johns Hopkins University School of Medicine, Baltimore, MD USA

[4]The Beckman Center for Cryo-EM at Johns Hopkins, Johns Hopkins University School of Medicine, Baltimore, MD USA

[5]Diana Helis Henry Medical Research Foundation, New Orleans, LA USA

[§]Equal Contribution

*Correspondence: Twomey@jhmi.edu (ECT); rhuganir@jhmi.edu (RLH)

Transmembrane AMPA receptor regulatory proteins (TARPs) are claudin-like proteins that tightly regulate AMPA receptors (AMPARs) and are fundamental for excitatory neurotransmission. We used cryo-electron microscopy (cryo-EM) to reconstruct the 36 kDa TARP subunit γ2 to 2.3 Å and reveal the structural diversity of TARPs. Our data reveals critical motifs that distinguish TARPs from claudins and define how sequence variations within TARPs differentiate subfamilies and their regulation of AMPARs.

Information transfer in the brain occurs at specialized cellular junctions known as synapses, which act as neuronal communication hubs[1]. Most synapses are glutamatergic, where a pre-synaptic neuron releases glutamate (Glu), and a post-synaptic neuron receives Glu. AMPARs in the post-synaptic membrane bind Glu and initiate depolarization of the post-synaptic neuron through their Glu-gated cation channels[1,2]. TARPs are auxiliary subunits that regulate the trafficking, gating kinetics, and pharmacology of AMPARs[2,3].

TARP regulatory subunits tightly regulate AMPAR function in the post-synaptic membrane, which is a critical aspect of the brain's ability to fine tune information processing[1–3]. There are six TARP subtypes (TARPγ2, γ3, γ4, γ5, γ7, γ8), split into type-I (TARPγ2, γ3, γ4, γ8) and type-II (TARPγ5, γ7) families. Generally, TARPs increase the conductance of AMPARs, but type-I TARPs slow desensitization and deactivation kinetics, while type-II TARPs appear to have a negative effect on gating when compared to type-I TARPs[2]. Furthermore, structural differences between TARPs in the same class underlie sensitivity to certain classes of drugs targeted to AMPAR-TARP complexes. Since the first TARP was identified a quarter century ago (TARPγ2, also known as stargazin)[4], TARPs have been recognized as an indispensable component of synaptic function[1,2]. Yet, the structural details of how TARPs regulate AMPARs remain ambiguous.

Cryo-EM studies of TARP subunits have advanced our understanding of TARP structure in the context of AMPAR complexes, but intermediate resolution has historically precluded *de novo* building of TARP structures[5–14]. X-ray crystallography structures of TARP homologs, such as claudins, have been indispensable for modeling TARPs[15]. Claudins are cellular junction proteins that form paracellular barriers between epithelial and endothelial cells and are functionally distinct from TARPs[16]. The reliance on claudin structures for TARP modeling has hampered identification

of distinct structural features that 1) differentiate TARPs from claudins and 2) explain the regulatory potential of TARPs for AMPARs. Here, we use cryo-EM to determine the structure of the prototypical TARP, TARPγ2. We identify new motifs in TARPγ2 that distinguish TARP classes from one another and further differentiate TARPs from Claudins. These structural features likely underlie modulatory effects exhibited by TARPs on AMPAR gating.

We reconstructed the 3D architecture of TARPγ2 to an overall resolution of 2.3 Å (2.0 Å – 2.5 Å locally; **Extended Data Fig. 1**). Our data enables us to build most of the transmembrane domain (TMD) and extracellular domain (ECD) *de novo* (**Fig. 1a**). The high resolution of our reconstruction enables identification of multiple distinct structural features in the TARPγ2 extracellular domain (ECD), which sits atop its tetraspanin transmembrane (TM) helical bundle comprised of transmembrane (TM) helices TM1-4 (**Fig. 1a**). The ECD is comprised of a five-stranded β-sheet and a single extracellular helix (ECH) that immediately precedes TM2. A previously identified disulfide bridge (DSB) between β3 (C67) and β4 (C77) strands in the ECD stabilizes the TARPγ2 ECD (**Fig. 1b**) and is conserved across all TARPs and the TARP-like claudins.

What makes TARPγ2, and all TARPs unique from claudins? We identify two new moieties in our reconstruction of TARPγ2 that distinguish TARPs from claudins. First, a π-π-π stack secures the TARPγ2 ECD atop the TARPγ2 TMD (**Fig. 1b**). This is formed by H60 (from β2), Y32 (TM1-β1 loop), and W178 (TM4). We term this the TARP cleat motif because it helps to fasten the ECD to the TMD. We also identified a second DSB in the ECD. This DSB, the loop anchor DSB, anchors the β1-β2 loop onto the β-sheet (**Fig. 1b**). The loop anchor DSB is made between C40 in the β1-β2 loop and C68 on β3. All together, these motifs rigidify the structure of TARPγ2 by providing additional structural interactions within the ECD and between the ECD and TMD (**Fig. 1c**).

How conserved are these motifs? The TARP cleat motif is conserved in all TARPs and the TARP-like subunit germline specific gene 1-like (GSG1L) (**Fig. 2a**) but absent from all claudins (**Extended Data Fig. 2**). We also tested for conservation of the cleat motif through AlphaFold2[17] structure prediction. This suggests that the TARP cleat motif is present in all mammalian TARPs (**Extended Data Fig. 3a**). Interestingly, while the TARP cleat motif is conserved in all TARPs, the loop anchor DSB is not (**Fig. 2a**). Structure prediction in AlphaFold2 (**Extended Data Fig. 3b**) also points to the loop anchor DSB being conserved in type-I TARPs but not in type-II TARPs. Thus, while our structure pointed us to look at the conservation of the cleat motif and loop anchor DSB, this was already predicted by AlphaFold2 (**Extended Data Fig. 3c**).

Surprisingly, the TARP cleat motif and loop anchor DSB are within previous TARP structures but not identified. Previously determined structures of TARPs are overall like our structure of TARPγ2 (**Fig. 2b**), and the loop anchor DSB is within structures of TARPγ3[18] and TARPγ8[11,12,19], and even previously published structures of TARPγ2[6]. However, it is absent, as expected, in the structure of the type-II TARP, TARPγ5[20,21] (**Fig. 2c**) and the TARP-like subunit GSG1L[7,20] (**Fig. 2c**). In contrast, the TARP cleat motif is conserved in all TARPγ3, γ5, and γ8 subunit structures as well as GSG1L[11,18,20] (**Fig. 2d**). Thus, we suggest expanding the type-II family of TARPs to include the GSG1L subunit. We hypothesize that these structural details and their conservation were previously missed because of a lack of structural resolution.

The dichotomy in β1-β2 loop organization between type-I and type-II TARPs has significant functional implications. For example, type-II TARPs lack the loop anchor DSB and have been observed to directly interact with AMPAR subunits that are in the A and C positions when they occupy the “X” auxiliary subunit site[7,20] (**Fig. 2e**). However, we expect that this is not possible for type-I TARPs in the X site given the presence of the loop anchor DSB, which locks in the β1-β2

loop in an orientation away from the A and C AMPAR subunit positions. However, if a type-I TARP occupies the "Y" TARP position (**Fig. 2e**), modulation of the AMPAR at subunit positions B or D by the β1-β2 loop is likely possible despite the loop anchor DSB, and is supported by observations in cryo-EM studies of type-I TARPs in complex with AMPARs[18]. Given the extreme conformational changes associated with AMPAR gating, the stark difference in the presence or absence of the loop anchor DSB within type-I TARPs versus type-II TARPs potentially explains differences in electrophysiology experiments between chimeric constructs of the β1-β2 loop in type-I and type-II TARPs.

The TARP cleat motif plays a significant role in distinguishing TARPs from claudins. Both TARPs and claudins share the same overall structural fold (i.e., tetraspanin with a five-stranded extracellular β-sheet). However, claudins have strong oligomerization properties, where they self-oligomerize to form paracellular barriers. A similar phenomenon has not been reported for TARP proteins. We hypothesize that the TARP cleat motif plays a role in preventing oligomerization in TARPs, enabling their complexation with AMPARs and other synaptic proteins.

In sum, we report the structure of TARPγ2, and how the newly identified structural features may account for critical functional differences between TARPs that tune AMPAR function throughout the central nervous system. In addition, we precisely define how TARPs are differentiated from claudins, which may explain the critical point of divergence between the structurally related proteins that are functionally distinct. Our findings provide a new framework for future studies to understand the function of TARPs and new foundations to target TARPs in structure-based drug design against AMPAR-related neurological disorders.

References

1. Diering, G. H. & Huganir, R. L. The AMPA Receptor Code of Synaptic Plasticity. *Neuron* **100**, 314–329 (2018).
2. Hansen, K. B. *et al.* Structure, Function, and Pharmacology of Glutamate Receptor Ion Channels. *Pharmacol Rev* **73**, 298–487 (2021).
3. Twomey, E. C., Yelshanskaya, M. V. & Sobolevsky, A. I. Structural and functional insights into transmembrane AMPA receptor regulatory protein complexes. *J Gen Physiol* **151**, 1347–1356 (2019).
4. Letts, V. A. *et al.* The mouse stargazer gene encodes a neuronal Ca2+-channel gamma subunit. *Nat Genet* **19**, 340–347 (1998).
5. Twomey, E. C., Yelshanskaya, M. V., Grassucci, R. A., Frank, J. & Sobolevsky, A. I. Elucidation of AMPA receptor-stargazin complexes by cryo-electron microscopy. *Science* **353**, 83–86 (2016).
6. Twomey, E. C., Yelshanskaya, M. V., Grassucci, R. A., Frank, J. & Sobolevsky, A. I. Channel opening and gating mechanism in AMPA-subtype glutamate receptors. *Nature* **549**, 60–65 (2017).
7. Twomey, E. C., Yelshanskaya, M. V., Grassucci, R. A., Frank, J. & Sobolevsky, A. I. Structural Bases of Desensitization in AMPA Receptor-Auxiliary Subunit Complexes. *Neuron* **94**, 569-580.e5 (2017).
8. Twomey, E. C., Yelshanskaya, M. V., Vassilevski, A. A. & Sobolevsky, A. I. Mechanisms of Channel Block in Calcium-Permeable AMPA Receptors. *Neuron* **99**, 956-968.e4 (2018).
9. Zhao, Y., Chen, S., Swensen, A. C., Qian, W.-J. & Gouaux, E. Architecture and subunit arrangement of native AMPA receptors elucidated by cryo-EM. *Science* **364**, 355–362 (2019).
10. Yu, J. *et al.* Hippocampal AMPA receptor assemblies and mechanism of allosteric inhibition. *Nature* **594**, 448–453 (2021).

11. Zhang, D. *et al.* Modulatory mechanisms of TARP γ8-selective AMPA receptor therapeutics. *Nat Commun* **14**, 1659 (2023).
12. Herguedas, B. *et al.* Mechanisms underlying TARP modulation of the GluA1/2-γ8 AMPA receptor. *Nat Commun* **13**, 734 (2022).
13. Chen, S. *et al.* Activation and Desensitization Mechanism of AMPA Receptor-TARP Complex by Cryo-EM. *Cell* **170**, 1234-1246.e14 (2017).
14. Zhao, Y., Chen, S., Yoshioka, C., Baconguis, I. & Gouaux, E. Architecture of fully occupied GluA2 AMPA receptor-TARP complex elucidated by cryo-EM. *Nature* **536**, 108–111 (2016).
15. Suzuki, H. *et al.* Crystal Structure of a Claudin Provides Insight into the Architecture of Tight Junctions. *Science* (2014).
16. Zihni, C., Mills, C., Matter, K. & Balda, M. S. Tight junctions: from simple barriers to multifunctional molecular gates. *Nat Rev Mol Cell Biol* **17**, 564–580 (2016).
17. Jumper, J. *et al.* Highly accurate protein structure prediction with AlphaFold. *Nature* **596**, 583–589 (2021).
18. Zhang, D. *et al.* Structural mobility tunes signalling of the GluA1 AMPA glutamate receptor. *Nature* 1–6 (2023) doi:10.1038/s41586-023-06528-0.
19. Zhang, D., Watson, J. F., Matthews, P. M., Cais, O. & Greger, I. H. Gating and modulation of a hetero-octameric AMPA glutamate receptor. *Nature* **594**, 454–458 (2021).
20. Klykov, O., Gangwar, S. P., Yelshanskaya, M. V., Yen, L. & Sobolevsky, A. I. Structure and desensitization of AMPA receptor complexes with type II TARP γ5 and GSG1L. *Mol Cell* **81**, 4771-4783.e7 (2021).
21. Gangwar, S. P. *et al.* Modulation of GluA2-γ5 synaptic complex desensitization, polyamine block and antiepileptic perampanel inhibition by auxiliary subunit cornichon-2. *Nat Struct Mol Biol* **30**, 1481–1494 (2023).
22. Emsley, P. & Cowtan, K. Coot: model-building tools for molecular graphics. *Acta Cryst D* **60**, 2126–2132 (2004).
23. Croll, T. I. ISOLDE: a physically realistic environment for model building into low-resolution electron-density maps. *Acta Crystallogr D Struct Biol* **74**, 519–530 (2018).
24. Liebschner, D. *et al.* Macromolecular structure determination using X-rays, neutrons and electrons: recent developments in Phenix. *Acta Cryst D* **75**, 861–877 (2019).
25. Williams, C. J. *et al.* MolProbity: More and better reference data for improved all-atom structure validation. *Protein Science* **27**, 293–315 (2018).
26. Pettersen, E. F. *et al.* UCSF ChimeraX: Structure visualization for researchers, educators, and developers. *Protein Science* **30**, 70–82 (2021).
27. Morin, A. *et al.* Collaboration gets the most out of software. *eLife* **2**, e01456 (2013).
28. Larkin, M. A. *et al.* Clustal W and Clustal X version 2.0. *Bioinformatics* **23**, 2947–2948 (2007).
29. Procter, J. B. *et al.* Alignment of Biological Sequences with Jalview. *Methods Mol Biol* **2231**, 203–224 (2021).

Methods

Construct design, protein expression, and purification

Mouse TARPγ2 was covalently fused to the rat AMPAR subunit GluA2, expressed, and purified as described in the preprint Hale, *et al*. *Biorxiv* 2023 (BIORXIV/2023/569057).

Cryo-EM Sample Preparation and Data Collection

Cryo-EM samples were prepared and collected as described in the preprint Hale, *et al*. *Biorxiv* 2023 (BIORXIV/2023/569057).

Image Processing

The initial stages of cryo-EM sample preparation were carried out as in the preprint Hale, *et al*. *Biorxiv* 2023 (BIORXIV/2023/569057). After generation of a 2.80 Å AMPAR-TARPγ2 local map (Extended Data Fig. 1a), symmetry expansion was used to refine the structure of TARPγ2. To achieve this, we applied C4 symmetry to the AMPAR-TARP particles (Extended Data Fig. 1a). We masked one TARPγ2 in the AMPAR-TARPγ2, then inverted this mask, and subtracted the inverted mask from all particle images. We then used the subtracted particle images, coupled with the original TARPγ2 mask (non-inverted) applied to the complete AMPAR-TARPγ2 complex cryo-EM map reference to refine the final cryo-EM reconstruction of TARPγ2 (Extended Data Fig. 1b).

Model building, refinement, and structural analysis

Coot[22] was used to build a polyalanine chain into TARPγ2 map. Bulky resides from sequence information were used to anchor the building. A previously determined structure of TARPγ2 (pdb 5WEO) and a structure predicted from AlphaFold2 (AlphaFold Protein Structure Database, #AF-O88602) were used as reference. Isolde[23] and Phenix[24] were used to refine the model. Quality of the model was assessed with MolProbity[25]. Visualizations and domain measurements were performed in ChimeraX[26]. Software was compiled and accessed via the SBGrid Consortium[27].

Sequence Analysis

All sequence alignments were done with ClustalW[28] and analyzed in Jalview[29].

Structure Prediction

TARP structure predictions of TARPγ2, γ3, γ4, γ5, γ7, γ8 of human, rat, mouse species were used from AlphaFold2[17]. For each TARP subunit structure prediction, the respective amino acids corresponding to the cleat motif and disulfide bridge were determined. Cleat motif measurements were taken by calculating the distance between the Cα's of histidine to tyrosine and Cα's of tyrosine to tryptophan. Calculations were performed using the Biopython.PDB package.

AlphaFold2 accession numbers of models: AF-Q9Y698, AF-A0JNG9, AF-O88602, AF-Q71RJ2, AF-Q9JJV5, AF-Q0VD05, AF-O60359, AF-Q8VHX0, AF-A0A3Q1LKG2, AF-Q9JJV4, AF-Q8VHW9, AF-Q9UBN1, AF-E1BEI3, AF-Q8VHW4, AF-Q8VHW8, AF-Q9UF02, AF-E1BIG3, AF-P62956, AF-P62957, AF-P62955, AF-Q8WXS5, AF-F1MV40, AF-Q8VHW2, AF-Q8VHW5.

Conflict of Interest

R.L.H. is scientific cofounder and Scientific Advisory Board (SAB) member of Neumora Therapeutics and SAB member of MAZE Therapeutics.

Data Availability

All cryo-EM reconstructions will be deposited into the Electron Microscopy Data Bank (EMDB) upon publication. All micrographs from the IS-1 and IS-2 datasets will be deposited into the Electron Microscopy Public Image Archive (EMPIAR) upon publication. All structural models generated from cryo-EM will be deposited in the Protein Data Bank upon publication.

Acknowledgements

We thank members of the Twomey and Huganir labs for insightful discussions. All cryo-EM data was collected at the Beckman Center for Cryo-EM at Johns Hopkins with assistance from D. Sousa and D. Ding.

Funding

E.C.T is supported by the Searle Scholars Program (Kinship Foundation #22098168) and the Diana Helis Henry Medical Research Foundation (#142548). R.L.H. is supported by National Institutes of Health (NIH) grants R01 NS036715 and R01 MH112152. W.D.H. is supported by NIH grant K99 MH132811.

Author Contributions

E.C.T. and R.L.H. supervised all aspects and planning of this research. E.C.T., A.M.R., and W.D.H. designed the project. E.C.T. and W.D.H. wrote the manuscript with input from all authors. W.D.H. prepared samples for cryo-EM, collected cryo-EM data, processed cryo-EM data, analyzed data, and built models with E.C.T. A.M.R. assisted with structural analysis, structure prediction, model building, data analysis, structural analysis, and in uncovering the conserved TARP motifs.

Cryo-EM data collection, refinement and validation statistics

	TARPγ2 (EMDB-xxxx) (PDB xxxx)
Data collection and processing	
Magnification	130,000x
Voltage (kV)	300
Electron exposure (e–/Å^2)	40
Defocus range (μm)	-1.0 – 2.6
Pixel size (Å)	0.93
Symmetry imposed	C1
Initial particle images (no.)	123,729
Final particle images (no.)	494,916
Map resolution (Å)	2.32
FSC = 0.143	
Map resolution range (Å)	2 – 4
Refinement	
Initial model used (PDB code)	N/A
Model resolution (Å)	2.3
FSC = 0.143	
Model resolution range (Å)	2.1 – 3.7
Map sharpening *B* factor (Å^2)	-54.8
Model composition	
Non-hydrogen atoms	2678
Protein residues	172
Ligands	0
B factors (Å^2)	
Protein	0.00/27.91/5.8
Ligand	N/A
R.m.s. deviations	
Bond lengths (Å)	0.013
Bond angles (°)	1.726
Validation	
MolProbity score	0.71
Clashscore	0
Poor rotamers (%)	1.44
Ramachandran plot	
Favored (%)	97.56
Allowed (%)	1.83
Disallowed (%)	0.61

Figure Legends

Figure 1. Structure of TARPγ2. a) Cryo-EM map of TARPγ2, colored rainbow from N-terminus, NT (blue) to C-terminus, CT (red). b) Extracellular portion of the TARPγ2 model showing the β3-β4 DSB, loop anchor DSB, and TARP cleat. c) Cartoon schematic of TARPγ2 structure highlighting key structural features that rigidify the entire ECD atop the tetraspanin TMD, colored as in panel a.

Figure 2. Conservation of structural features among TARP family members. a) Multiple sequence alignment demonstrating the relative conservation of the TARP Cleat Motif, β3-β4 DSB, and Loop Anchor DSB between TARP family members. Loop Anchor DSB is unique to type-I and excluded from type-II TARPs. b) Alignment of TARPγ2 structure with other TARP family members (TARPγ3, PDB: 8C2H; TARPγ5, PDB: 7RZ5; TARPγ8, PDB: 8AYN; GSG1L, PDB: 7RZ9). c) Zoomed in view of TARP extracellular domains illustrating differing orientations in the β1-β2 loops. d) View of the TARP cleat motif illustrating conservation among all TARP family members. e) Model of predicted β1-β2 loop orientations between type-I and type-II TARPs illustrating distinct potential contacts between TARP subtypes and AMPARs.

Extended Data Figure 1. Details of TARPγ2 data processing workflow. a) Symmetry expansion of the GluA2-TARPγ2 assembly (from Hale et al., 2023, *BioRxiv*). b) Masking scheme for isolating symmetry-expanded TARPγ2. c) TARPγ2 cryo-EM map colored by local resolution *right:* surface of TARPγ2 reconstruction, *left:* cutaway showing resolution inside the map. d) Gold Standard Fourier Shell Correlation and Guinier Plots for TARPγ2. e) Model fit to cryo-EM map of the four TARPγ2 TM helices. f) Cryo-EM map around the TARP Cleat motif and the Loop Anchor DSB.

Extended Data Figure 1 2. Multiple sequence alignment of TARPs, GSG1L and Claudins. Multiple sequence alignments of TARPs, GSG1L and all members of the Claudin family. The TARPs and GSG1L are distinguished from Claudins by the presence of the TARP cleat motif while the β3-β4 DSB is conserved among both TARPs and Claudins.

Extended Data Figure 3. AlphaFold structure prediction of TARPs. a) Conservation of TARP cleat residues in bovine, rat, mouse, and human TARPs. TARPγ2 from this study is pointed out. b) Loop anchor DSB vs. β3-β4 DSB distances. The TARP cleat is predicted to be present in all TARPs. Type-II TARPs are excluded from panel b because the loop anchor DSB is predicted to be absent in type-II TARPs. These findings are summarized in panel c.

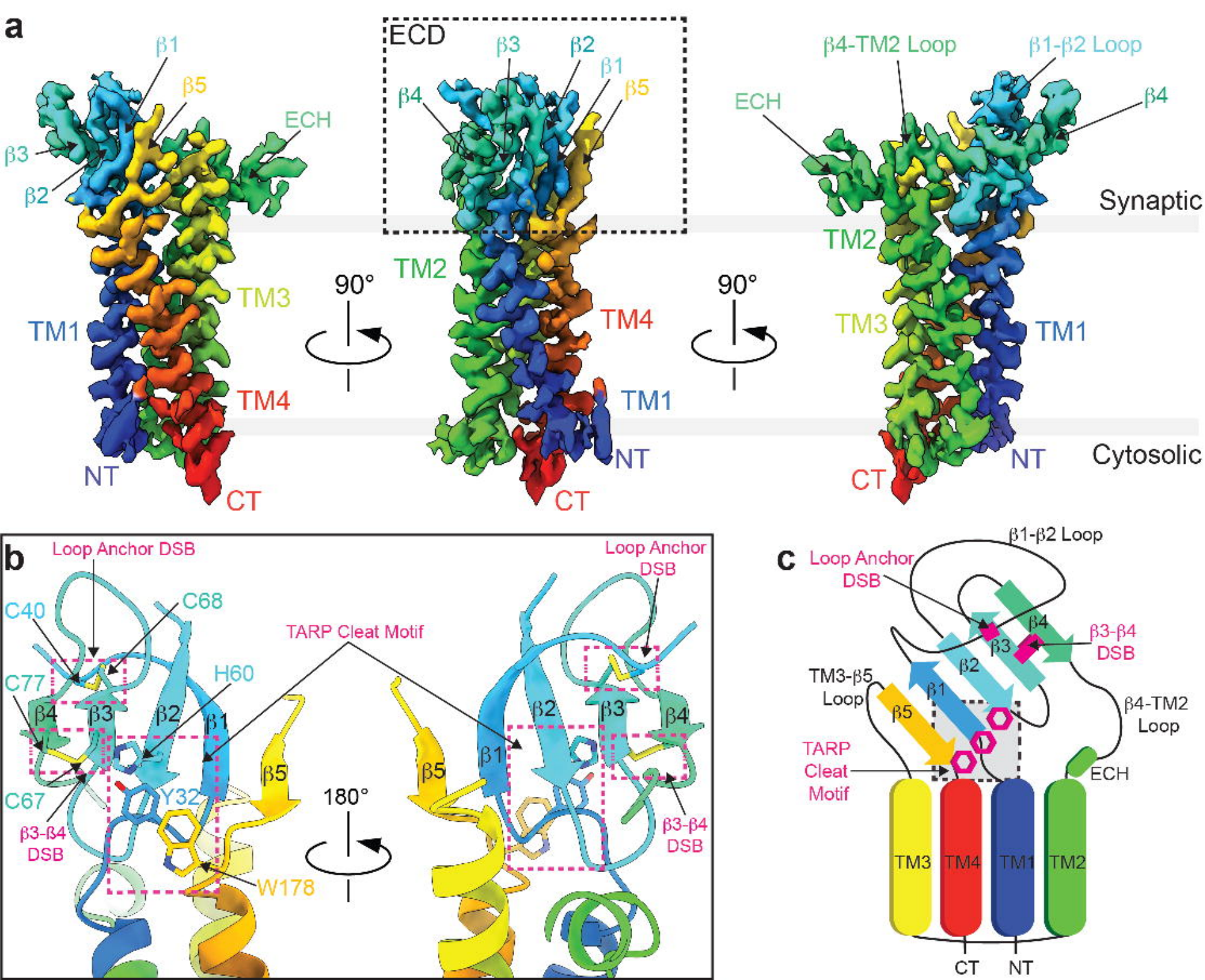
a
ECD
β1
β5
ECH
β3
β2
TM3
TM1
TM4
NT
CT
β3
β2
β1
β5
β4
TM2
TM4
TM1
NT
CT
90°
90°
β4-TM2 Loop
β1-β2 Loop
ECH
β4
Synaptic
TM2
TM3
TM1
NT
CT
Cytosolic
b
Loop Anchor DSB
Loop Anchor DSB
C40
C68
TARP Cleat Motif
C77
H60
β4
β3
β2
β1
β5
C67
Y32
β3-β4 DSB
W178
180°
β5
β1
β2
β3
β4
β3-β4 DSB
c
β1-β2 Loop
Loop Anchor DSB
β4
β3
β3-β4 DSB
β2
β1
TM3-β5 Loop
β5
β4-TM2 Loop
TARP Cleat Motif
ECH
TM3
TM4
TM1
TM2
CT
NT

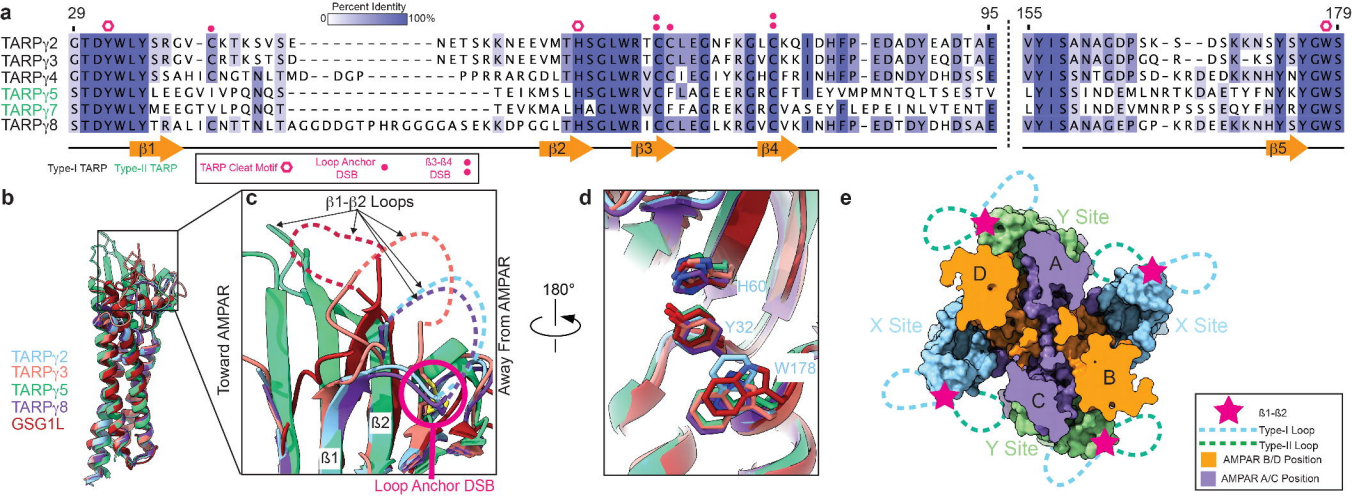
a
Percent Identity
0
100%
29
95
155
179
TARPγ2 GTDYWLYSRGV-CKTKSVSE----------NETSKKNEEVMTHSGLWRTCCLEGNFKGLCKQIDHFP-EDADYEADTAE VYISANAGDPSK-S--DSKKNSYSYGWS
TARPγ3 GTDYWLYSRGV-CRTKSTSD----------NETSRKNEEVMTHSGLWRTCCLEGAFRGVCKKIDHFP-EDADYEQDTAE VYISANAGDPGQ-R--DSK-KSYSYGWS
TARPγ4 GTDYWLYSSAHICNGTNLTMD--DGP--------PPRRARGDLTHSGLWRVCCIEGIYKGHCFRINHFP-EDNDYDHDSSE VYISSNTGDPSD-KRDEDKKNHYNYGWS
TARPγ5 STDYWLYLEEGVIVPQNQS----------TEIKMSLHSGLWRVCFLAGEERGRCFTIEYVMPMNTQLTSESTV LYISSINDEMLNRTKDAETYFNYKYGWS
TARPγ7 STDYWLYMEEGTVLPQNQT----------TEVKMALHAGLWRVCFFAGREKGRCVASEYTLEPEINLVTENTE LYISSINDEVMNRPSSSEQYFHYRYGWS
TARPγ8 STDYWLYTRALICNTTNLTAGGDDGTPHRGGGGASEKKDPGGLTHSGLWRICCLEGLKRGVCVKINHFP-EDTDYDHDSAE VYISANAGEPGP-KRDEEKKNHYSYGWS
β1
β2
β3
β4
β5
Type-I TARP
Type-II TARP
TARP Cleat Motif
Loop Anchor DSB
β3-β4 DSB
b
TARPγ2
TARPγ3
TARPγ5
TARPγ8
GSG1L
c
β1-β2 Loops
Toward AMPAR
Away From AMPAR
β2
β1
Loop Anchor DSB
d
180°
H60
Y32
W178
e
Y Site
X Site
X Site
Y Site
A
B
C
D
β1-β2
Type-I Loop
Type-II Loop
AMPAR B/D Position
AMPAR A/C Position

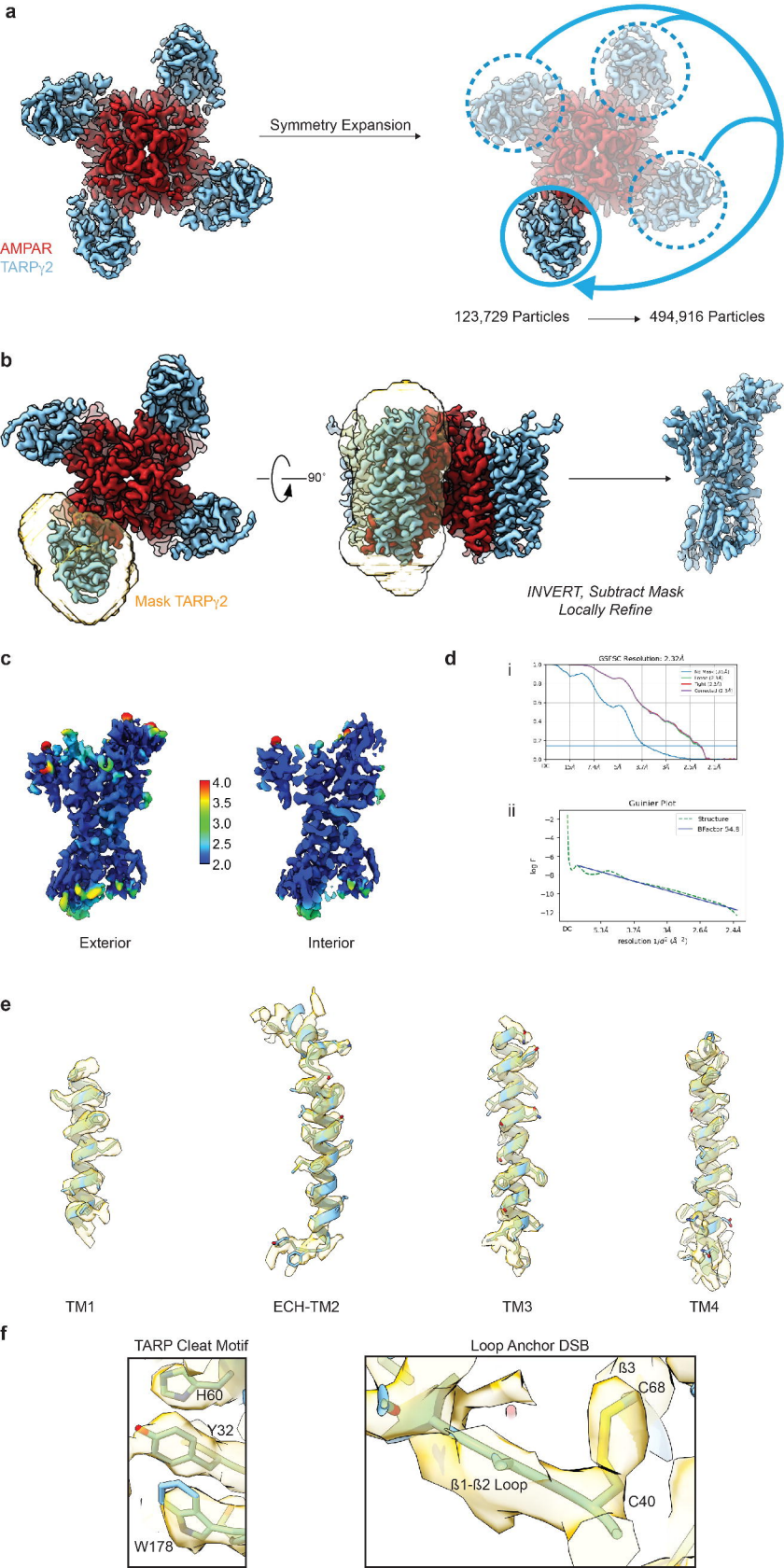
a
AMPAR
TARPγ2
Symmetry Expansion
123,729 Particles
494,916 Particles
b
90°
Mask TARPγ2
INVERT, Subtract Mask
Locally Refine
c
4.0
3.5
3.0
2.5
2.0
Exterior
Interior
d
i
ii
Guinier Plot
Structure
BFactor 54.8
log I
resolution 1/d² (Å⁻²)
e
TM1
ECH-TM2
TM3
TM4
f
TARP Cleat Motif
H60
Y32
W178
Loop Anchor DSB
ß3
C68
ß1-ß2 Loop
C40

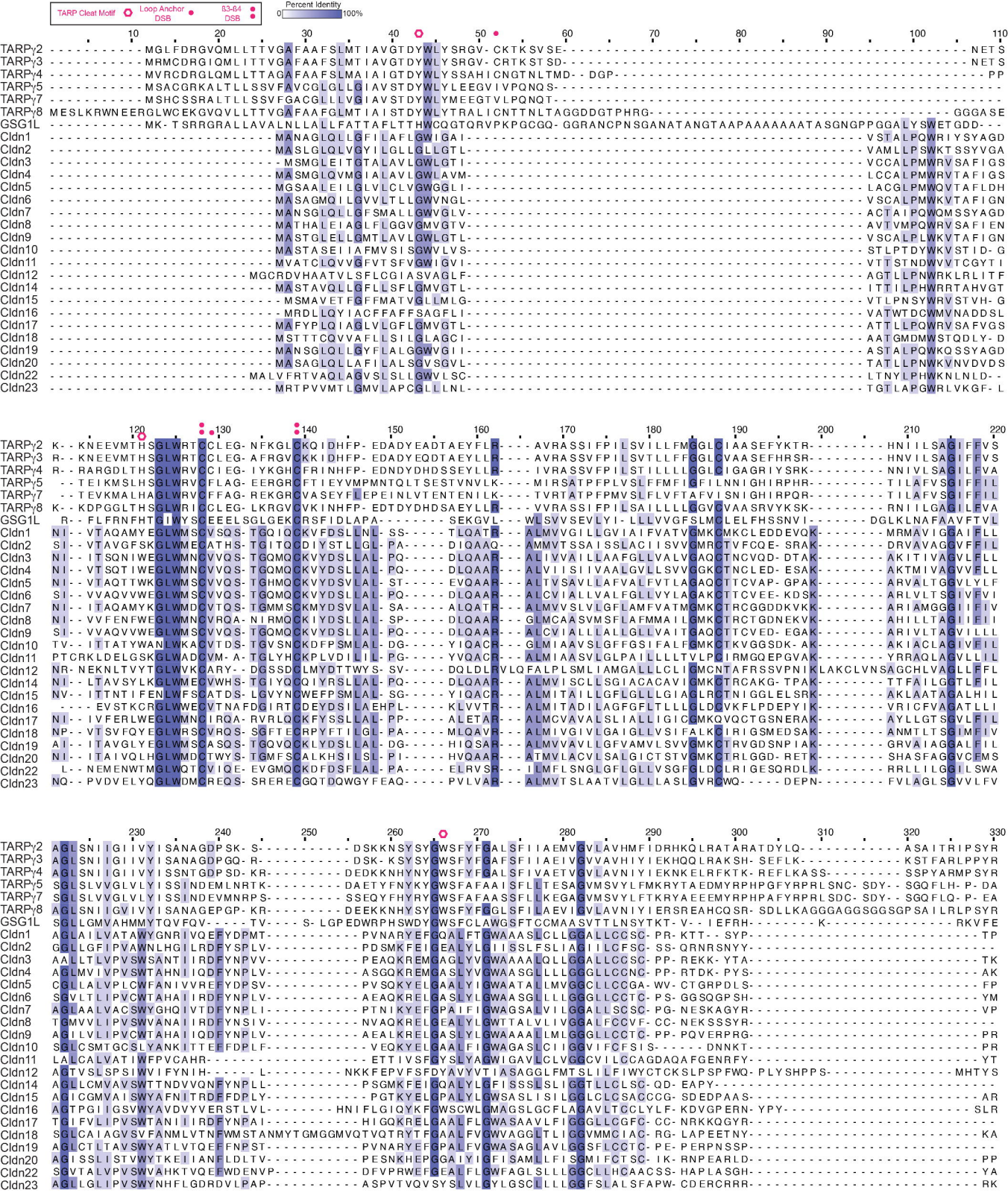
TARP Cleat Motif
Loop Anchor DSB
β3-β4 DSB
Percent Identity
0
100%
TARPγ2
TARPγ3
TARPγ4
TARPγ5
TARPγ7
TARPγ8
GSG1L
Cldn1
Cldn2
Cldn3
Cldn4
Cldn5
Cldn6
Cldn7
Cldn8
Cldn9
Cldn10
Cldn11
Cldn12
Cldn14
Cldn15
Cldn16
Cldn17
Cldn18
Cldn19
Cldn20
Cldn22
Cldn23

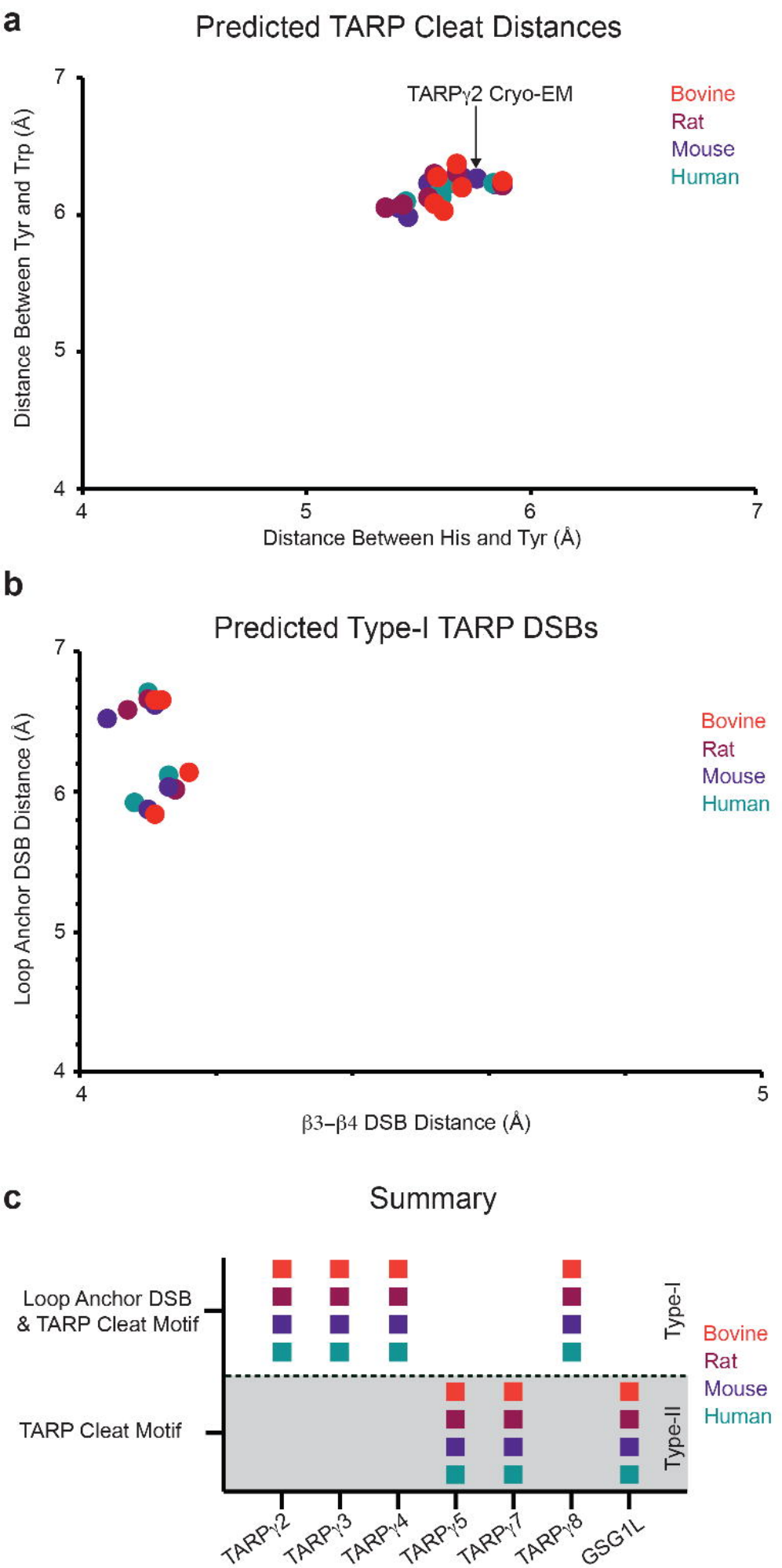
a
Predicted TARP Cleat Distances
TARPγ2 Cryo-EM
Bovine
Rat
Mouse
Human
Distance Between Tyr and Trp (Å)
Distance Between His and Tyr (Å)
4
5
6
7
b
Predicted Type-I TARP DSBs
Loop Anchor DSB Distance (Å)
β3–β4 DSB Distance (Å)
c
Summary
Loop Anchor DSB & TARP Cleat Motif
TARP Cleat Motif
Type-I
Type-II
TARPγ2
TARPγ3
TARPγ4
TARPγ5
TARPγ7
TARPγ8
GSG1L